

# Quantum fields in a cold atomic simulator: relaxation and phase locking in tunnel-coupled 1D bosonic quasi-condensates

Bence Fitos<sup>1, 2, \*</sup> and Gábor Takács<sup>1, 3, †</sup>

<sup>1</sup>*Department of Theoretical Physics, Institute of Physics,*

*Budapest University of Technology and Economics, H-1111 Budapest, Műegyetem rkp. 3.*

<sup>2</sup>*HUN-REN-BME-BCE Quantum Technology Research Group, Institute of Physics,*

*Budapest University of Technology and Economics, Műegyetem rkp. 3., H-1111 Budapest, Hungary*

<sup>3</sup>*BME-MTA Momentum Statistical Field Theory Research Group, Institute of Physics,*

*Budapest University of Technology and Economics, Műegyetem rkp. 3., H-1111 Budapest, Hungary*

(Dated: December 8, 2025)

We consider a prime example of simulating interacting relativistic QFT with cold atoms: the realisation of the sine-Gordon model by tunnel-coupled quasi-1D Bose gases. While experiments have shown that it can realise the sine-Gordon model in equilibrium, studies of non-equilibrium dynamics have revealed a phase-locking behaviour that stands in contrast to predictions from sine-Gordon field theory. Here, we examine a one-dimensional field-theoretic model of the system and find that the phase-locking behaviour can be understood in terms of the presence of the longitudinal harmonic trap, and that the additional degrees of freedom known to be present in the experiment do not appear to play a significant role. Therefore, the experimental setup provides a good simulator of the sine-Gordon quantum field theory, even out of equilibrium, if the inhomogeneous background induced by the trap is taken into account. Furthermore, our results support the idea that modifying the longitudinal trap to a box shape should result in agreement with standard sine-Gordon dynamics. The main remaining open issues are to account for 3D corrections and model the effect of the boundaries.

## CONTENTS

I. Introduction	1
II. Model and methodology	2
A. The effective 1D description	2
B. The tunnel coupling	5
C. Lattice discretisation	5
D. The truncated Wigner approximation	6
III. Breaking down the model	7
A. The main scenarios	7
B. Further refinements	7
1. Finite temperature	7
2. Particle number variance	8
IV. The full dynamics in the experimental parameter regime	9
A. Simulations	9
B. Timescales	9
V. Simplified models	11
A. Fitting functions	11
B. Josephson frequency	11
C. Relaxation time	11
VI. Conclusions	11

## Acknowledgments

14

## References

14

## A. Summary of model parameters

17

## I. INTRODUCTION

Feynman's idea of using quantum systems to simulate other quantum systems [1], particularly quantum field theories, has found a promising avenue in experiments with ultracold atoms [2], which leverage the high degree of control and tunability offered by ultracold atomic systems to mimic the behaviour of quantum particles and fields, and offer a pathway to explore phenomena beyond the reach of classical computation. Engineering and manipulating isolated quantum systems has now become routine in experiments with trapped ultracold atoms [3–10]. In particular, they provide access to the out-of-equilibrium dynamics of quantum systems, which has been at the forefront of research in recent years [11–14].

Here we consider the sine-Gordon model, which is a paradigmatic interacting integrable quantum field theory that describes the low-energy physics of numerous physical systems [15–23]. An interesting feature of the model is its integrability, which provides exact results for numerous quantities, ranging from scattering amplitudes and form factors to expectation values of local observables [24–26].

The sine-Gordon model can be realised experimentally with two Josephson-coupled one-dimensional bosonic quasi-

\* [fitos5bence@gmail.com](mailto:fitos5bence@gmail.com)

† [takacs.gabor@ttk.bme.hu](mailto:takacs.gabor@ttk.bme.hu)

condensates<sup>1</sup> [7, 27, 30], whereas ultra-cold atoms are trapped in an elongated double-well potential, effectively limiting the physics to one spatial dimension. Bosonisation of the one-dimensional description of the many-body system [30], leads to a sine-Gordon model realised by the relative phase between the condensates, which is weakly coupled to a Luttinger liquid accounting for their common (average) phase. The latter coupling breaks integrability; however, equilibrium correlation functions agree well with sine-Gordon predictions [27, 31], indicating that in thermal equilibrium the coupled condensates can be regarded as a good quantum simulator of the sine-Gordon quantum field theory.

Out-of-equilibrium dynamics can be investigated using the paradigmatic protocol of quantum quench [32, 33], which involves preparing the system in an equilibrium state and then suddenly changing some physical parameter, e.g., a coupling in a Hamiltonian. In the coupled condensates, a natural protocol involves splitting a single one-dimensional condensate, imprinting a relative phase between them, and then switching on the tunnel coupling. Theoretical computations based on pure sine-Gordon dynamics predict a rephasing [34–37], in which the relative phase of the condensates relaxes to a finite value. In contrast, the experiment found a rapid phase locking [38] between the condensates, which can be parameterised in terms of a two-mode model extended with a dissipative term [39, 40]. The main experimental findings can be captured using a stochastic Gross-Pitaevskii description [41], which, however, steps outside the framework of the quantum field theoretic (sine-Gordon) description. The alternative approach, involving a self-consistent Hartree-Fock approximation [42–44], is not applicable in the parameter regime relevant to the experiment, which involves a significantly higher number of particles than those used in the model calculation.

In this paper, we consider the dynamics of the system in the effective coupled sine-Gordon-Luttinger field theory description, using the so-called truncated Wigner approximation [45–47]. In fact, this has already been applied to

the sine-Gordon model, resulting in universal rephasing dynamics [34]. The validity of the TWA method can be confirmed by using Hamiltonian truncation [48, 49], which, however, cannot reach the experimentally relevant parameter regime. Here we take into account the longitudinal trapping potential, as well as the coupling between the sine-Gordon and Luttinger degrees of freedom and demonstrate that this approach captures the phase locking dynamics as illustrated in Fig. I.1. For qualitative comparison with the experiment, the parameters are selected according to Ref. [38].

The outline of the paper is as follows. Section II reviews the derivation of the effective field theoretical description for the coupled condensates and the implementation of the truncated Wigner approximation. In Section III, we consider three crucial ingredients of the model: the nonlinearity inherent in the sine-Gordon self-interaction, the spatial inhomogeneity resulting from the trapping potential, and the coupling between the relative (sine-Gordon) and common (Luttinger) modes. Section IV presents the results for the full dynamics in the experimental parameter regime. In section V, we analyse the scaling of the Josephson frequency and relaxation time of the relative phase as a function of various input parameters of the experiment and compare the findings to previous results. In addition, we compare our results to the leading order behaviour of small quenches described by a free massive boson approximation of the sine-Gordon field. Finally, we present our conclusions in Section VI. We also added a summary of useful relations between different parameters in Appendix A.

## II. MODEL AND METHODOLOGY

### A. The effective 1D description

In this section, we describe the quasi-one-dimensional model of a single elongated bosonic quasi-condensate. We start from the grand canonical Hamiltonian of a three-dimensional interacting Bose gas:

$$H = \int d^3\vec{r} \Psi^\dagger(\vec{r}) \left( -\frac{\hbar^2}{2m} \nabla^2 + V(\vec{r}) - \mu \right) \Psi(\vec{r}) + \int d^3\vec{r} d^3\vec{r}' \Psi^\dagger(\vec{r}) \Psi^\dagger(\vec{r}') U_{\text{eff}}(\vec{r} - \vec{r}') \Psi(\vec{r}') \Psi(\vec{r}),$$

$$[\Psi(\vec{r}), \Psi^\dagger(\vec{r}')] = \delta(\vec{r} - \vec{r}')$$
(II.1)

<sup>1</sup> Alternative cold atom realisations can be found in Refs. [2, 22, 27, 28]; additional proposals include realisations via quantum circuits [19] or coupled spin chains [29].

where  $m$  is the atomic mass,  $V(\vec{r})$  is the 3D trapping potential and  $\mu$  is the chemical potential. For low temperatures, the effective interaction  $U_{\text{eff}}$  can be approximated by a delta potential

$$U_{\text{eff}}(\vec{r} - \vec{r}') = \frac{4\pi\hbar^2}{m} a_s \delta(\vec{r} - \vec{r}')$$
(II.2)

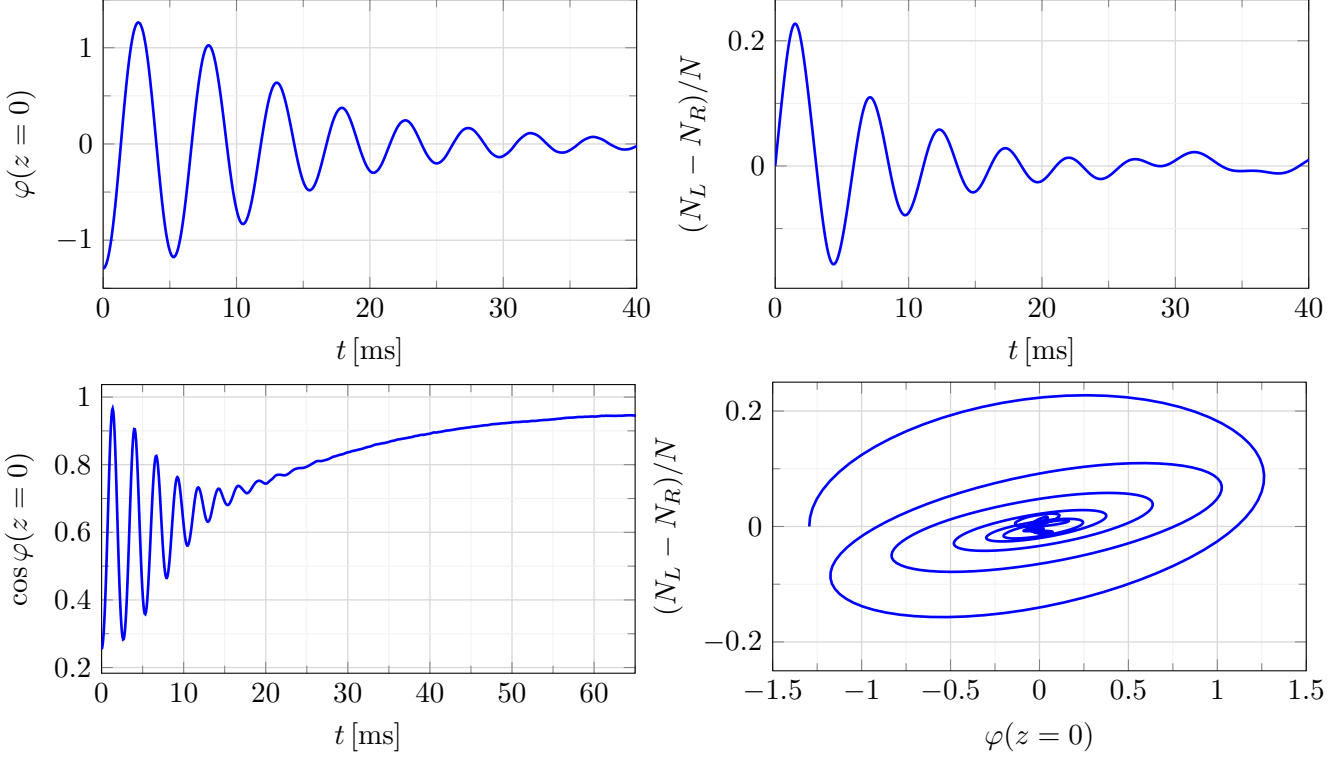


Figure I.1: TWA results of the phase and the total particle number difference of a Josephson quench. We also illustrated the evolution of  $\cos \varphi$  signalling phase locking with  $\langle \cos \varphi \rangle_{\text{eq}} \approx 0.945$ . The expectation value of  $\varphi$  is taken in the middle of the condensate ( $z = 0$ ). Parameters:  $N = 3300$ ,  $\omega_{\parallel} = 2\pi \cdot 12 \text{ s}^{-1}$ ,  $J/(2\pi\hbar) = 19.0 \text{ Hz}$ ,  $T = 0$ ,  $\sigma_N = 300$ ,  $\varphi_0 = -1.3(2)$ .

characterised by the  $s$ -wave scattering length  $a_s$ .

Switching on a radial trapping potential, e.g. of the form

$$\frac{1}{2}m\omega_{\perp}^2(x^2 + y^2) \quad (\text{II.3})$$

in the  $xy$  plane leads to an elongated condensate, which can be modelled as an effectively one-dimensional Lieb-Liniger gas

---


$$H = \int dz \psi^{\dagger}(z) \left( -\frac{\hbar^2}{2m} \partial_z^2 + V(z) - \mu + \frac{g_{1\text{D}}}{2} \psi^{\dagger}(z) \psi(z) \right) \psi(z), \quad (\text{II.4})$$


---

where the effective one-dimensional coupling can be expressed in terms of the  $s$ -wave scattering length and the frequency  $\omega_{\perp}$  of the transversal trapping potential [50]

$$g_{1\text{D}} \approx \frac{2\hbar^2 a_s}{ml_{\perp}^2} \left( 1 - 1.036 \frac{a_s}{l_{\perp}} \right)^{-1}. \quad (\text{II.5})$$

Here  $l_{\perp} = \sqrt{\hbar/(m\omega_{\perp})}$  is the transverse oscillator length associated with the frequency  $\omega_{\perp}$  of the radial confining potential, and  $a_s$  the three-dimensional  $s$ -wave scattering length of the atoms. In the weak interaction regime  $a_s \ll l_{\perp}$

the result simplifies  $g_{1\text{D}} \approx 2\hbar\omega_{\perp}a_s$ .

We assume that the system is in the quasi-condensate regime where the density of the condensate can be considered a classical function  $\rho_0(z)$  dressed up by relatively smaller quantum fluctuations. To obtain a low-energy effective theory, it is useful to introduce the Madelung representation of the field

$$\psi(z) = e^{i\varphi(z)} \sqrt{\rho_0(z) + \delta\rho(z)}, \quad (\text{II.6})$$

where  $\hat{\varphi}(z)$  and  $\delta\hat{\rho}(z)$  are real-valued fields. The classical background density profile  $\rho_0(z)$  satisfies the Gross-

Pitaevskii equation

$$\left(-\frac{\hbar^2}{2m}\partial_z^2 + V(z) - \mu + g_{1D}\rho_0(z)\right)\sqrt{\rho_0(z)} = 0, \quad (\text{II.7})$$

where the chemical potential  $\mu$  is fixed by the total number of particles

$$N = \int dz \rho_0(z). \quad (\text{II.8})$$

In the experimental setup, the condensate is further confined in the  $z$  direction by the quadratic potential

$$V(z) = \frac{1}{2}m\omega_{||}^2 z^2, \quad (\text{II.9})$$

where  $\omega_{||} \ll \omega_{\perp}$ . Neglecting the kinetic term in (II.7) (local density approximation) gives the Thomas–Fermi density profile

$$\rho_0(z) = n_0 \left(1 - \frac{z^2}{R_{\text{TF}}^2}\right), \quad (\text{II.10})$$

where

$$R_{\text{TF}} = \frac{L}{2}, \quad n_0 = \frac{3N}{2L}, \quad (\text{II.11})$$

with  $L$  giving the full length in the  $z$  direction.

To the leading order approximation in the density fluctuations  $\delta\rho$ , the system is then described by an inhomogeneous Luttinger–liquid Hamiltonian [51]

$$H_{\text{TLL}} = \frac{\hbar}{2\pi} \int dz \left( \nu_N(z) (\pi\delta\rho)^2 + \nu_J(z) (\partial_z\varphi)^2 \right) \quad (\text{II.12})$$

where the density and phase stiffness are given by [52, 53]

$$\begin{aligned} \nu_N(z) &= \frac{1}{\pi\hbar} \left. \frac{\partial\mu}{\partial\rho_0} \right|_{\rho_0=\rho_0(z)} \approx \frac{g_{1D}}{\pi\hbar} \\ \nu_J(z) &= \frac{\pi\hbar\rho_0(z)}{m}. \end{aligned} \quad (\text{II.13})$$

where the first approximation holds in the weakly interacting regime

$$\gamma = \frac{mg_{1D}}{\hbar^2 n_{1D}} \ll 1. \quad (\text{II.14})$$

The Hamiltonian can be written in the form

$$H_{\text{TLL}} = \frac{\hbar c_0}{2} \int dz \left( \frac{\pi}{K_0} \delta\rho^2 + f(z) \frac{K_0}{\pi} (\partial_z\varphi)^2 \right), \quad (\text{II.15})$$

where

$$n_0 = \rho_0(z=0) \quad (\text{II.16})$$

is the density,

$$f(z) = \frac{\rho_0(z)}{n_0} \quad (\text{II.17})$$

is the dimensionless density profile,

$$c_0 = \sqrt{\frac{g_{1D}n_0}{m}} \quad (\text{II.18})$$

is the sound velocity, and

$$K_0 = \pi\hbar\sqrt{\frac{n_0}{mg_{1D}}} \quad (\text{II.19})$$

is the (dimensionless) Luttinger parameter, and the index 0 indicates that all of them are specified by their local values at the midpoint  $z = 0$ .

The spectrum of the quadratic Hamiltonian (II.15) can be obtained in terms of decoupled bosonic modes satisfying the classical equation of motion in terms of the renormalised field  $\phi(z) = \sqrt{K_0}/\pi \varphi(z)$

$$-\partial_t^2\phi + \partial_z(f\partial_z\phi) = 0, \quad (\text{II.20})$$

for which the solutions can be written in the form

$$\phi_{n\pm}(t, z) = e^{\pm i\omega_n t} Z_n(z), \quad (\text{II.21})$$

where

$$\partial_z(f\partial_z Z_n) = -\omega_n^2 Z_n, \quad (\text{II.22})$$

where we choose all the  $Z_n$ ’s as real-valued functions, which form an orthonormal basis

$$\int_{L/2}^{L/2} dz Z_n(z) Z_m(z) = \delta_{nm}. \quad (\text{II.23})$$

Then  $\phi$  can be decomposed into eigenmodes

$$\phi(t, z) = \sum_n \frac{Z_n(z)}{\sqrt{2\omega_n}} (a_n e^{-i\omega_n t} + a_n^\dagger e^{i\omega_n t}), \quad (\text{II.24})$$

where  $a_n$  and  $a_n^\dagger$  are bosonic creation and annihilation operators, from which the Hamiltonian becomes

$$H_{\text{TLL}} = \hbar c_0 \sum_n \omega_n a_n^\dagger a_n + \text{const}. \quad (\text{II.25})$$

In the case of the Thomas–Fermi density profile (II.10) we have  $f(z) = 1 - 4z^2/L^2$  and the  $Z_n$  functions can be expressed by Legendre polynomials:

$$Z_n(z) = \sqrt{\frac{2n+1}{L}} P_n\left(\frac{z}{L/2}\right), \quad (\text{II.26})$$

with the corresponding frequencies given by

$$\omega_n = \frac{1}{L} \sqrt{(2n+1)^2 - 1}. \quad (\text{II.27})$$

Note that the issue of the boundary conditions is rather non-trivial. Naively, particle number conservation implies Neumann boundary conditions ( $\partial_z\phi = 0$  at the boundaries)

at both ends of the system. However, since  $f(z)$  vanishes at the boundaries, we can at most prescribe regularity (finiteness) for  $Z_n$  at the boundaries. Indeed, it turns out that the general solution of the differential equation is a linear combination of Legendre functions of the first and second kind. Dropping the latter, irregular one and matching the frequencies leads to the solutions above.

The decomposition of the field into eigenmodes can be written as

$$\begin{aligned}\tilde{\phi}_n &= \int dz Z_n(z) \phi(z), \\ \tilde{\Pi}_n &= \int dz Z_n(z) \Pi(z),\end{aligned}\quad (\text{II.28})$$

with the inverse transformations

$$\begin{aligned}\phi(z) &= \sum_n Z_n(z) \tilde{\phi}_n, \\ \Pi(z) &= \sum_n Z_n(z) \tilde{\Pi}_n.\end{aligned}\quad (\text{II.29})$$

### B. The tunnel coupling

The experimental setup corresponds to coupling two quasi-condensates  $\psi_{1,2}(z)$  via a tunnelling Hamiltonian

$$H_I = -J \int dz \left( \psi_1^\dagger(z) \psi_2(z) + \psi_2^\dagger(z) \psi_1(z) \right). \quad (\text{II.30})$$

Using the Madelung representation Eq. (II.6) for of  $\psi_{1,2}$  shows that the coupling between the two condensates depends on the relative phase  $\varphi_1(z) - \varphi_2(z)$ . Therefore, we introduce the *relative* and *common* degrees of freedom

$$\begin{aligned}\varphi^r(z) &:= \varphi_1(z) - \varphi_2(z), \\ \varphi^c(z) &:= \frac{\varphi_1(z) + \varphi_2(z)}{2}, \\ \delta\rho^r(z) &:= \frac{\delta\rho_1(z) - \delta\rho_2(z)}{2}, \\ \delta\rho^c(z) &:= \delta\rho_1(z) + \delta\rho_2(z).\end{aligned}\quad (\text{II.31})$$

To the lowest order in density fluctuation, the relative mode is described by the sine–Gordon model with the interaction Hamiltonian

$$H_I^{(0)} = -2J \int dz \rho_0(z) \cos(\varphi^r(z)), \quad (\text{II.32})$$

while the common mode remains an independent Luttinger liquid. Higher-order corrections couple the relative to the

common mode, and the next-to-leading order gives the term

$$H_I^{(1)} = -J \int dz \delta\rho^c(z) (\cos(\varphi^r(z)) - 1). \quad (\text{II.33})$$

### C. Lattice discretisation

The inhomogeneous Luttinger Hamiltonian (II.12) can be discretised by a lattice  $z_j = ja$  with lattice spacing  $a$ , and its dimensionless version (corresponding to condensate  $s = 1, 2$ ) can be written in the form

$$\begin{aligned}\tilde{H}_{\text{TLL},s}^\# &= \\ \frac{1}{2} \sum_j \left( \Pi_{s,j}^2 + \frac{f(z_j) + f(z_{j+1})}{2} (\phi_{s,j+1} - \phi_{s,j})^2 \right),\end{aligned}\quad (\text{II.34})$$

where

$$\begin{aligned}\tilde{H}^\# &= \frac{a}{\hbar c_0} H^\#, \\ \Pi_{s,j} &= \sqrt{\frac{\pi}{K_0}} a \delta\rho_s(z_j), \quad \phi_{s,j} = \sqrt{\frac{K_0}{\pi}} \varphi_s(z_j).\end{aligned}\quad (\text{II.35})$$

To characterise the tunnel coupling interaction suitably, we switch to relative and common degrees of freedom

$$\begin{aligned}\phi_j^r &= \frac{1}{\beta_r} \varphi^r(z_j), \quad \Pi_j^r = a \beta_r \delta\rho^r(z_j), \\ \phi_j^c &= \frac{1}{\beta_c} \varphi^c(z_j), \quad \Pi^c = a \beta_c \delta\rho^c(z_j),\end{aligned}\quad (\text{II.36})$$

where

$$\beta_r = \sqrt{\frac{2\pi}{K_0}}, \quad \beta_c = \sqrt{\frac{\pi}{2K_0}}. \quad (\text{II.37})$$

The Luttinger Hamiltonian in terms of the relative and common degrees of freedom takes the same form as Eq. (II.34), while the dimensionless lattice regularised interaction terms corresponding to (II.32) and (II.33) can be expressed as

$$\begin{aligned}\tilde{H}_I^{(0)\#} &= \frac{2g L n_0}{N_s} \sum_j f(z_j) \cos(\beta_r \phi_j^r), \\ \tilde{H}_I^{(1)\#} &= \frac{g}{N_s} \sum_j \frac{\Pi_j^c}{\beta_c} (\cos(\beta_r \phi_j^r) - 1),\end{aligned}\quad (\text{II.38})$$

where  $N_s = L/a$  is the number of lattice sites, and

$$g = 2\pi \frac{J}{2\pi\hbar} \frac{L}{c_0}. \quad (\text{II.39})$$

Combining the free and interacting parts, the complete lattice regularised dimensionless Hamiltonian takes the form

$$\begin{aligned}
\tilde{H}^\# &= \tilde{H}_{\text{TLL},1}^\# + \tilde{H}_{\text{TLL},2}^\# + \tilde{H}_I^{(0)\#} + \tilde{H}_I^{(1)\#} \\
&= \sum_j \left\{ \frac{1}{2} \left[ (\Pi_j^r)^2 + \frac{f(z_j) + f(z_{j+1})}{2} (\phi_{j+1}^r - \phi_j^r)^2 \right] + \frac{1}{2} \left[ (\Pi_j^c)^2 + \frac{f(z_j) + f(z_{j+1})}{2} (\phi_{j+1}^c - \phi_j^c)^2 \right] \right. \\
&\quad \left. - \frac{2gLn_0}{N_s^2} f(z_j) \cos(\beta_r \phi_j^r) - \frac{g}{N_s} \frac{\Pi_j^c}{\beta_c} [\cos(\beta_r \phi_j^r) - 1] \right\}.
\end{aligned} \tag{II.40}$$

#### D. The truncated Wigner approximation

To simulate the quasi-condensate in the experimentally relevant parameter regime, we adopt a powerful semiclassical method, the truncated Wigner approximation (TWA) [54, 55], which is particularly suitable for calculating out-of-equilibrium expectation values. The TWA is based on the one-to-one mapping between quantum operators and ordinary functions defined in the (classical) phase space: for an arbitrary operator  $\hat{\Omega}$  we define the *Weyl symbol*

$$\Omega_W(\mathbf{x}, \mathbf{p}) = \int d\mathbf{x}' \left\langle \mathbf{x} - \frac{\mathbf{x}'}{2} \middle| \hat{\Omega} \middle| \mathbf{x} + \frac{\mathbf{x}'}{2} \right\rangle e^{i\mathbf{p}\mathbf{x}'}, \tag{II.41}$$

where  $|\mathbf{x}\rangle$  are the eigenstates of the position operator  $\hat{\mathbf{x}}$ . In particular, the Weyl symbol of the density matrix with a suitable normalisation is called the Wigner function

$$W(\mathbf{x}, \mathbf{p}) = \frac{1}{(2\pi\hbar)^{N_s}} \int d\mathbf{x}' \left\langle \mathbf{x} - \frac{\mathbf{x}'}{2} \middle| \hat{\rho} \middle| \mathbf{x} + \frac{\mathbf{x}'}{2} \right\rangle e^{i\mathbf{p}\mathbf{x}'}, \tag{II.42}$$

where  $N_s$  is the dimension of the  $\mathbf{x}$  and  $\mathbf{p}$  vectors.

The trace of a product of two operators can be expressed as a phase space integral of their Weyl symbols. In particular, for an expectation value, we get

$$\langle \hat{\Omega} \rangle = \int d\mathbf{x} d\mathbf{p} W(\mathbf{x}, \mathbf{p}) \Omega_W(\mathbf{x}, \mathbf{p}). \tag{II.43}$$

To incorporate time evolution, we approximate the trajectories of the phase space points with the classical paths

$$\langle \hat{\Omega} \rangle_{\text{TWA}}(t) = \int d\mathbf{x}_0 d\mathbf{p}_0 W(\mathbf{x}_0, \mathbf{p}_0) \Omega_W(\mathbf{x}(t), \mathbf{p}(t)), \tag{II.44}$$

where  $\mathbf{x}(t)$  and  $\mathbf{p}(t)$  are the solutions of the classical equations of motion with the initial conditions  $\mathbf{x}(0) = \mathbf{x}_0$  and  $\mathbf{p}(0) = \mathbf{p}_0$ , respectively. The truncated Wigner approximation can be systematically derived as the leading order of a systematic expansion of the Keldysh path integral for quantum fields [54, 55]. Here, we follow the exposition in [48], to which we refer for further details on the implementation.

In the context of the coupled condensate system, the canonically conjugate classical variables are  $\{\phi_j^r, \Pi_j^r\}_{j=1, \dots, N_s}$  and  $\{\phi_j^c, \Pi_j^c\}_{j=1, \dots, N_s}$ . The pre-quench

state is the uncoupled condensate,  $J = 0$ , corresponding to the dimensionless Hamiltonian  $\tilde{H}_{\text{pre}}^\# = \tilde{H}_{\text{TLL},1}^\# + \tilde{H}_{\text{TLL},2}^\#$ . The pre-quench Hamiltonian is quadratic and can be diagonalized with the linear transformation  $\{(\phi_j^\alpha, \Pi_j^\alpha)\} \rightarrow \{(\tilde{\phi}_n^\alpha, \tilde{\Pi}_n^\alpha)\}$ ,  $\alpha = r, c$  described in Eq. (II.28).<sup>2</sup> Note that, for a lattice regularised theory, the eigenmode decomposition (II.28) transformation is established by an orthogonal matrix, which is the set of eigenvectors of the lattice regularisation of the differential operator in Eq. (II.22).

The ground state Wigner function is a Gaussian in each transformed mode  $\{(\tilde{\phi}_n^\alpha, \tilde{\Pi}_n^\alpha)\}$ , which allows for Monte-Carlo sampling. For  $n \neq 0$ , the standard deviations of the  $n$ th mode  $(\tilde{\phi}_n^\alpha, \tilde{\Pi}_n^\alpha)$  is given by

$$\begin{aligned}
\sigma_{\tilde{\phi}_n^\alpha} &= \frac{1}{\sqrt{2a\omega_n}}, \\
\sigma_{\tilde{\Pi}_n^\alpha} &= \sqrt{\frac{a\omega_n}{2}}.
\end{aligned} \tag{II.45}$$

The zero mode energy is zero ( $\omega_0 = 0$ ), therefore the ground state Wigner function is a uniform distribution on  $[0, 2\pi\sqrt{N_s}/\beta_\alpha]$  in variable  $\tilde{\phi}_0^\alpha$  and a  $\delta$  function (centred at 0) in variable  $\tilde{\Pi}_0^\alpha$ .

The experimental quenching protocol sets the total relative phase

$$\varphi_0^r = \frac{1}{L} \int dz \varphi^r(z) = \frac{\beta_r}{\sqrt{N_s}} \tilde{\phi}_0^r \tag{II.46}$$

with some standard deviation  $\sigma_{\varphi_0}$ . Therefore, instead of a uniform distribution, we incorporate the experimentally given zero mode of the relative phase  $\tilde{\phi}_0^r$  into the Wigner function: a normal distribution centred at  $\sqrt{N_s} \varphi_0^r / \beta_r$  with standard deviation

$$\sigma_{\tilde{\phi}_0^r} = \frac{\sqrt{N_s}}{\beta_r} \sigma_{\varphi_0}. \tag{II.47}$$

The corresponding conjugate variable  $\tilde{\Pi}_0^r$  is chosen to be a Gaussian centred around 0 with standard deviation minimising the Heisenberg inequality:

$$\sigma_{\tilde{\Pi}_0^r} = \frac{\beta_r}{2\sqrt{N_s} \sigma_{\varphi_0}}. \tag{II.48}$$

<sup>2</sup> We define an additional normalization factor  $\sqrt{a}$  to eliminate the dimension of the  $Z_n$  functions.

The TWA simulation consists of taking a Monte-Carlo sample of initial values from which the real space functions are obtained via the inverse transformation Eq. (II.29). The TWA simulation then consists of computing the classical time evolution from these initial conditions using the interacting Hamiltonian  $J \neq 0$ . Observables are computed by averaging the values obtained from individual trajectories. The Monte-Carlo error of these averages is estimated from the standard deviation of the data at each time point. The TWA has several significant advantages, including numerical stability and broad scalability, which enable negligible MC error even with limited computational resources. We note that TWA also allows for computations at finite temperature  $k_B T = 1/\beta$ , where each (non-zero) mode in the Wigner function remains Gaussian with a broadened standard deviation

$$\sigma^{(\beta)} = \sigma \cdot \sqrt{\frac{e^{\beta\omega} + 1}{e^{\beta\omega} - 1}}. \quad (\text{II.49})$$

### III. BREAKING DOWN THE MODEL

#### A. The main scenarios

To achieve a systematic understanding of the coupled condensate system, we dissect the model along its primary characteristics. We begin by examining the linearised sine-Gordon model on a homogeneous background. The full model is then constructed incrementally, with each step introducing a new aspect of the full model. For each of these refinements, we analyse its specific impact on the system's dynamics.

The subsequent analysis focuses on three crucial characteristics of the model:

- **Non-linearity:** This concerns the validity of the quadratic approximation for the cosine potential in accurately describing the system's behaviour.
- **Inhomogeneity:** We examine the impact of the quadratic longitudinal trapping potential (resulting in an approximate Thomas-Fermi density profile) on the dynamics, contrasting it with a simple flat-bottom potential.
- **Common-mode coupling:** We examine the influence of the subleading interaction term, Eq. (II.33), which couples the common and relative phase modes.

For a systematic comparison of these effects, we explore all  $2^3 = 8$  combinations obtained by activating them. Throughout the different settings, we keep the local physical parameters constant at the midpoint  $z = 0$ . Figure III.1 presents the resulting dynamics for the relative phase defined at the midpoint

$$\langle \cos \varphi \rangle(t) = \langle \cos \varphi^r(z = 0, t) \rangle, \quad (\text{III.1})$$

obtained using experimentally relevant parameters. Notably, the eight different scenarios lead to qualitatively distinct dynamic behaviours.

Our main finding is that the phase relaxation  $\langle \cos \varphi \rangle(t) \rightarrow \approx 1$  can be attributed to the inhomogeneity resulting from the presence of the quadratic longitudinal trapping potential. Regardless of the other two settings, in the presence of an inhomogeneous background, the relative phase  $\langle \cos \varphi \rangle(t)$  system approaches  $\approx 1$  on the timescale of  $2\pi/\omega_{\parallel}$  determined by the longitudinal trap. However, once  $\langle \cos \varphi \rangle(t)$  reached its peak, revivals appear, which decrease its value. Nevertheless, there is a well-defined plateau before the appearance of revivals when the  $\langle \cos \varphi \rangle(t)$  is stabilised around a value close to 1, indicating phase locking. In this regard, we note that even the expectation value of  $\langle \cos \varphi \rangle$  does not exactly equal 1 even in the (zero temperature) sine-Gordon vacuum [26] due to quantum fluctuations of the phase field  $\varphi$ . Even more deviation from 1 is expected after a quantum quench, which injects finite energy density into the system. Therefore, even in phase locking, we expect residual fluctuations in the relative phase, leading to  $\langle \cos \varphi \rangle(t)$  relaxing to a value slightly less than 1.

Depending on the parameter regime, both nonlinearity and common-mode coupling can play a role in suppressing these revivals; however, for the experimentally relevant regime, the effect of common-mode coupling on the dynamics turned out to be negligible.

The nonlinearity of the cosine interaction is another important characteristic of the model. It is obviously relevant for large  $\varphi_0$  values of the initial phase. Furthermore, it also turns out to play an important role in smoothing the Josephson oscillations for general values of the other parameters.

#### B. Further refinements

To make our analysis more realistic, we considered several further refinements, including a finite temperature and uncertainty in the initial particle number loaded into the system when initiating the individual experimental runs.

##### 1. Finite temperature

We considered runs at finite temperature and found that it leads to an additional damping in the relaxation of  $\langle \varphi^r(t) \rangle \rightarrow 0$ . Additionally, it also decreases the asymptotic value of the phase  $\langle \cos \varphi^r(t) \rangle$  (c.f. Fig. III.2). Since the experimentally observed phase locking was quite robust, we expect that the temperature of the relative degrees of freedom was considerably smaller than the energy scales governing phase locking. Therefore, in order to keep things simple, from now on, we consider simulations at zero temperature (if not indicated otherwise).

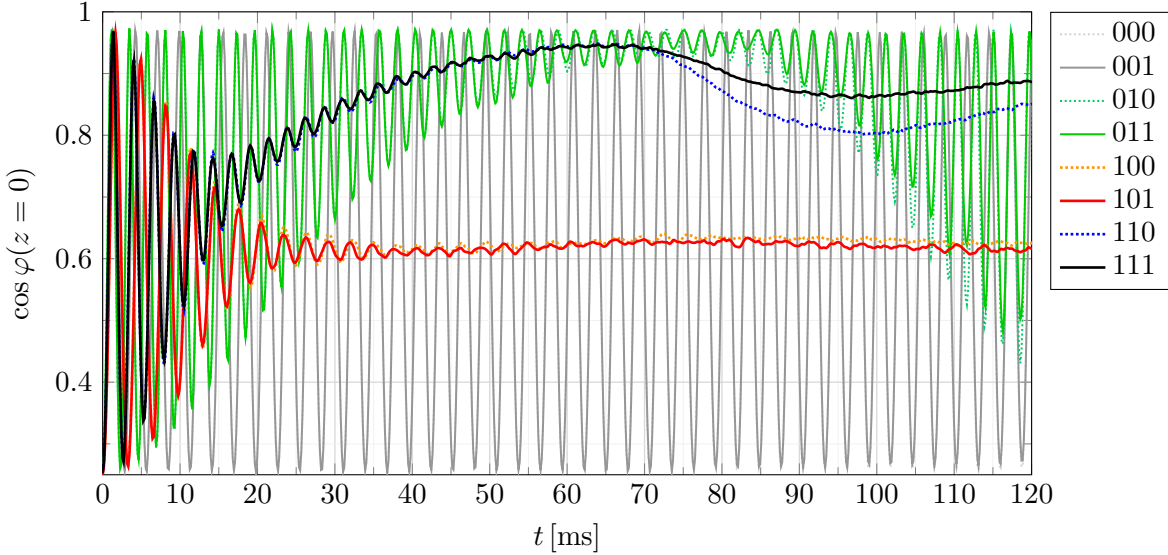


Figure III.1: Eight scenarios compared. The binary codes indicate the presence or absence of the three characteristics of the model: nonlinearity, inhomogeneity, and common-mode coupling. Parameters:  $N = 3300, J/(2\pi\hbar) = 19.0 \text{ Hz}, T = 0.0 \text{ nK}, \varphi_0^r = -1.3, \sigma_{\varphi_0^r} = 0.2, \sigma_N = 0$ .

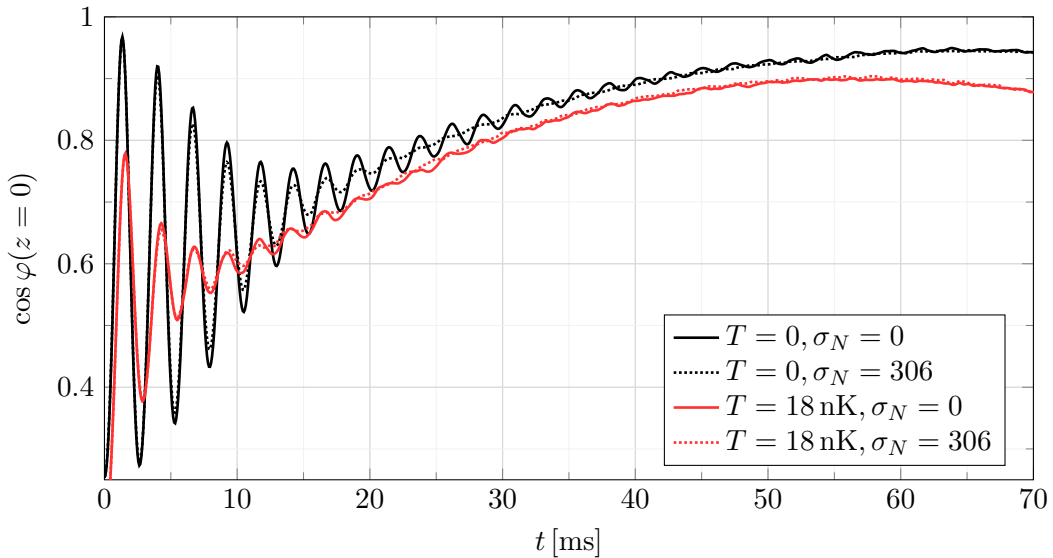


Figure III.2: Analysing the effect of finite temperature and the fluctuation of the initial number of atoms considering the  $\cos \varphi^r$  expectation value. Parameters:  $N = 3300, J/(2\pi\hbar) = 19.0 \text{ Hz}, \varphi_0^r = -1.3, \sigma_{\varphi_0^r} = 0.2$ .

## 2. Particle number variance

Another refinement is to consider the uncertainty of the initial parameters. Here we limit ourselves to the uncertainty of the initial number of particles  $N$ . In the experiment, the data points are calculated as an average of multiple single runs; therefore, the fluctuation of initial parameters results in an additional damping due to decoherence.

In contrast to thermal fluctuation, the decoherence resulting from the variance of the initial particle number leads

to damping only in  $\langle \varphi^r(t) \rangle$ . The uncertainty of the initial parameters does not change the expected variance of  $\varphi^r$  and therefore does not dampen the expectation value of  $\langle \cos \varphi^r \rangle$ .

The simplest way to characterise the distribution of the atom number  $N$  is given by a Gaussian distribution. However, it is not clear how the standard deviation  $\sigma_N$  is related to the total number of particles. Moreover, one may also consider a post-selection approach (neglecting runs with too large particle deviation, cf. [41]); however, a sharp cut-

off is experimentally unrealistic and results in an unphysical  $\approx \text{sinc}(\tilde{\omega}t)$  modulation. Based on these considerations, we consider a simple Gaussian distribution, assuming that the standard deviation is clearly defined by the corresponding experimental setup.

## IV. THE FULL DYNAMICS IN THE EXPERIMENTAL PARAMETER REGIME

### A. Simulations

We also ran a full simulation in the parameter regime relevant for the experiment [38]. The results are shown in Fig. I.1. From the experimental settings, we fixed the following values for the parameters

$$\begin{aligned} N &= 3300, \quad \sigma_N = 300, \\ \omega_{||} &= 2\pi \cdot 12 \text{ s}^{-1}, \quad J/(2\pi\hbar) = 19 \text{ Hz}, \\ \varphi_0^r &= -1.3, \quad \sigma_{\varphi_0^r} = 0.2, \end{aligned} \quad (\text{IV.1})$$

for the average number of atoms and its variance, the longitudinal trap frequency, the Josephson coupling<sup>3</sup>, and the initial phase, respectively. The temperature is set to  $T = 0$  as explained in Subsection III B 1, and the only variable for which we had a freedom of choice is the initial time offset to match the start of the experimental data taking.

We found that with a single choice of this time offset, the simulated curves accurately capture the characteristics of the experimental data. Additionally, we also displayed the theoretical evolution of the expectation value of the cosine of the relative phase. The reason is that the relaxation of the average to zero does not necessarily signify phase locking, which also requires its variance to approach zero. The evidence for the latter is provided by the fact that the cosine of the phase relaxes to a value close to 1.

### B. Timescales

The behaviour of the system can be understood on three different hierarchical timescales.

The first is the timescale of the Josephson oscillations  $1/f_J$ , for which the dynamics of the relative mode is well described by the sine–Gordon model in a homogeneous potential. We observe no qualitative differences (other than a renormalisation of the Josephson frequency) compared to the inhomogeneous model and the model including the common-mode coupling (see Fig. III.1).

The next timescale is the relaxation time corresponding to  $\langle \cos \varphi \rangle(t) \rightarrow \approx 1$ . Since phase locking is the result of

the trap, the time until the system reaches phase locking is characterised by  $\omega_{||}$ . As is apparent from Fig. I.1, this timescale is approximately the same as the relaxation time of the oscillations in  $\langle \varphi \rangle(t) \rightarrow 0$ . We investigate the dependence of the relaxation time on experimental parameters in the next section.

The sine–Gordon model is well-known to be integrable on a homogeneous background. At the same time, it does not show a full relaxation to a phase-locked state; rather, it only has a (universal) rephasing dynamics, for which the expectation value of the relative phase approaches a non-zero value [34, 37]. The inhomogeneity induced by the trap breaks integrability, and so one naturally expects a profound change in the relaxation dynamics. However, the detailed connection between the breaking of integrability and phase locking remains unclear at this stage. Furthermore, we observe that the coupling to the common mode does not play a significant role at this timescale, although it also breaks integrability.

The third timescale is the one of the revivals that appear, which is when the coupling to the common-mode can become relevant by further suppressing revivals in the inhomogeneous sine–Gordon model. This feature can be understood by noting that the coupling to the common mode is suppressed by the particle density, which is high in the middle region of the condensate but approaches zero near the ends. Therefore, the common-mode coupling has a negligible effect on the dynamics in the middle region of the condensate for short times, but it can have a large effect on the reflection from the boundaries and, therefore, the revivals. However, due to the density approaching zero at the boundaries, the field-theoretic description has a limited validity in its neighbourhood; therefore, a more detailed and realistic description of this regime requires further research.

## V. SIMPLIFIED MODELS

In this section, we analyse the scaling of the relaxation time  $\tau$  and the Josephson frequency  $\omega_J$  of  $\varphi^r(t, z = 0)$  as a function of the input parameters of the model.

### A. Fitting functions

To define  $\tau$  and  $\omega_J$ , we fitted  $\varphi(t) \equiv \varphi^r(t, z = 0)$ <sup>4</sup> with a damped oscillation

$$\varphi_{\text{fit}}(t) = \varphi_{\text{fit}}^0 e^{-t/\tau} \sin(\omega_J t + \vartheta_0), \quad (\text{V.1})$$

which is the exact analytic form of the leading order behaviour of small quenches (with one-particle contributions)

<sup>3</sup> The Josephson coupling is determined from the frequency of the oscillations.

<sup>4</sup> To avoid edge effects, we considered the local observable in the centre and time evolution before revivals reach the middle point.

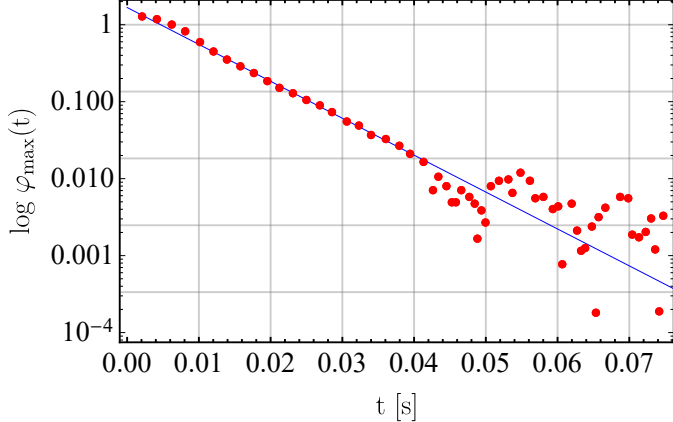


Figure V.1: Local extrema of  $\varphi(t)$  on the semi-log axis (red dots). The blue line indicates the plateau corresponding to the long-living excitations. Parameters:  $T = 0$  nK,  $\varphi_0^r = -1.3$ ,  $\sigma_{\varphi_0^r} = 0.2$ ,  $\sigma_N = 300$ ,  $N = 3300$ ,  $J/(2\pi\hbar) = 31.2$  Hz.

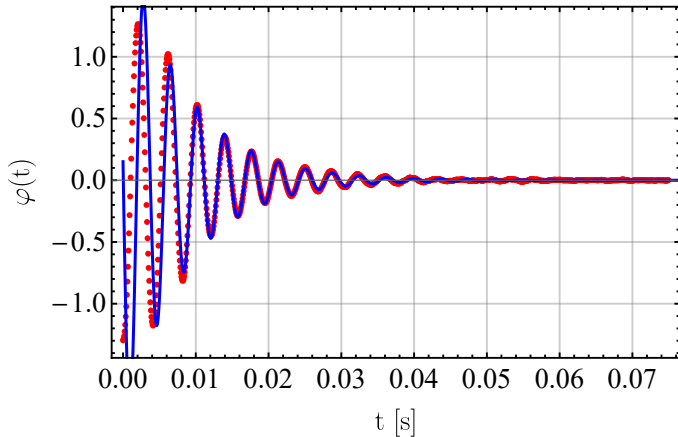


Figure V.2: The  $\varphi(t)$  expectation value from the TWA simulation (red dots) and the fitted function Eq. (V.1) (blue line). Parameters:  $T = 0$  nK,  $\varphi_0^r = -1.3$ ,  $\sigma_{\varphi_0^r} = 0.2$ ,  $\sigma_N = 300$ ,  $N = 3300$ ,  $J/(2\pi\hbar) = 31.2$  Hz, fit results:  $\varphi_{\text{fit}}^0 = 2.09$ ,  $\omega_J = 1694$  s $^{-1}$ ,  $\tau = 8.10$  ms.

in massive quantum field theories [56]. The sinusoidal form can be obtained from a leading order form factor expansion on the pre-quench basis [57, 58], while a resummation of higher order terms (in an expansion using the post-quench basis) elucidates the origin of the exponential damping [59, 60].

We remark that the start of the quench does not provide a good fit even with non-linear model functions (e.g. for the two-mode model used in Ref. [38]). We only found robust fitting by considering the long-living excitations. As the amplitude of the long-living excitations becomes relatively small, we can use the fit function in Eq. (V.1) coming from a leading order small density approximation.

We first smoothed the result of the TWA simulation,  $\varphi(t)$ , and identified its zeros, local minima, and maxima.

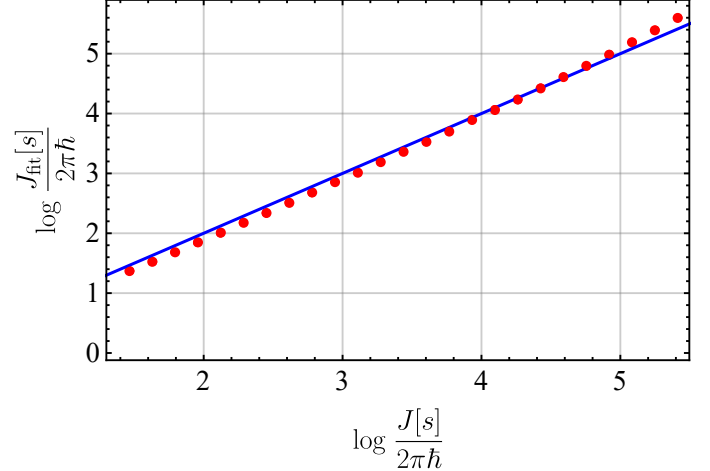


Figure V.3: The fitted Josephson coupling  $J_{\text{fit}}$  as a function of the input coupling of the simulation  $J$  (red dots) compared to the identity function (blue line). Parameters:  $N = 3300$ ,  $T = 0$  nK,  $\varphi_0^r = -1.3$ ,  $\sigma_{\varphi_0^r} = 0.2$ ,  $\sigma_N = 300$ .

Observing the absolute values of the local extremal points on the semi-log plot, we can identify a decreasing plateau corresponding to the relaxation of long-living oscillations (c.f. Fig. V.1). To capture this regime, we fit Eq. (V.1) between the 3rd and 10th periods of Josephson oscillations. A typical fit is illustrated in Fig. V.2.

We also briefly analysed the conjugate variable  $\Pi(t, z = 0)$ , which corresponds to the local particle imbalance in the centre. The total particle number difference between the two condensates is extrapolated from this quantity as

$$n := \frac{N_L - N_R}{N_L + N_R} \approx \frac{4}{3} \frac{N_s}{N} \frac{\Pi_r(0)}{\beta_r}, \quad (\text{V.2})$$

which is obtained by assuming  $\delta\rho^r(z)/\rho_0(z) \approx \delta\rho^r(0)/\rho_0(0)$ . This approximation is not necessarily valid in every regime; nevertheless, it provides a way to calculate an effective Josephson coupling ( $J_{\text{fit}}$ , see Eq. (V.4)) which turns out to be a consistent proxy in the experimental domain of parameters.

Assuming  $\tau \gg 1/\omega_J$ , the particle imbalance becomes

$$n_{\text{fit}}(t) = n_{\text{fit}}^0 e^{-t/\tau} \cos(\omega_J t + \vartheta_0). \quad (\text{V.3})$$

Considering  $\{\varphi(t, 0), \Pi(t, 0)\}$  as a single-mode oscillator, the effective Josephson coupling can be expressed in terms of the fitted parameters

$$J_{\text{fit}} = \frac{\hbar\omega_J}{2} \frac{n_{\text{fit}}^0}{\varphi_{\text{fit}}^0}. \quad (\text{V.4})$$

We found that the effective Josephson coupling ( $J_{\text{fit}}$ ) is in notable agreement with the raw input parameter of the simulation  $J$  (see Fig. V.3), which confirms the self-consistency of our approach.

## B. Josephson frequency

Next, we analysed the Josephson frequency  $\omega_J$ . It is natural to compare this to the simplest quantum field theoretical approximation of the leading-order behaviour. For small quenches, the middle region of the condensate can be approximated with the free (homogeneous) massive boson. The parameters of this free boson are chosen such that the local parameters (particle density  $n$ , sound velocity  $c$ , Luttinger parameter  $K_0$ ) match the corresponding ones at the midpoint  $z = 0$ . The initial state is modelled as a coherent state corresponding to an initial expectation value  $\varphi_0$ . It is then straightforward to express the oscillation frequency with the parameters of the condensate as

$$\omega_J = \sqrt{\frac{8\pi^2 \tilde{J} c_0 n_0}{K_0}} = 2\pi \left( \frac{3^2 \tilde{J}^3 N^2 g_{1D}^2 \omega_{||}^2 m}{2^4 \pi^3 \hbar^3} \right)^{1/6}, \quad (\text{V.5})$$

where  $\tilde{J} = J/(2\pi\hbar)$ . We check this analytic result against the simulation results obtained in our model.<sup>5</sup> Fig. V.4 shows the frequency of the Josephson oscillations as a function of the Josephson coupling, the number of atoms, and the strengths of the trapping potential, compared to the theoretical prediction (V.5). We found good agreement between the theoretical prediction and the simulated results.

The agreement between the theoretical prediction by the linearised model and the simulation proved to be robust even for large initial phase differences, indicating that the dynamics is dominated by low-energy sine-Gordon breather quasi-particles, which are well-approximated within the linearised model, after an initial transient which is omitted from the fitting.

## C. Relaxation time

Next, we considered the damping time  $\tau$  at different parameter settings (see Fig. V.5). We found that the damping time only shows a slight oscillatory dependence on the initial global phase  $\varphi_0$ . On the other hand, we found a decreasing tendency of  $\tau$  as a function of the Josephson coupling  $J$ , the total number of particles  $N$  and the strengths of the trapping potential. Assuming a power-law dependence, we fitted a line to the logarithmic plot to extract the corresponding exponents. We found that the relaxation time scaled with the power  $-1/2$  of the Josephson coupling  $J$ , and the power  $-1/3$  of the particle number  $N$  and longitudinal trap strength  $\omega_{||}$ . For the case of the transversal potential strength,  $\omega_{\perp}$ , the exponent is not absolutely clear (somewhere between  $1/4$  and  $1/3$ ); a wider logarithmic range should be covered to give a more accurate

<sup>5</sup> The Josephson frequency is obtained by fitting the aforementioned model to the simulated data.

result. Unfortunately, the parameters cannot be changed indefinitely, as one must obtain a reasonable number of Josephson oscillations before revivals reach back from the edges.

Our results for the scaling of  $\tau$  as a function of the parameters  $J$  and  $N$  deviate from the results given in previous studies [38, 41]. In this respect, we emphasise that our simulations are based on an effectively one-dimensional model, which does not account for all 3D phenomena. One such correction is the local swelling of the condensate when the linear particle density is increased, which results in a position-dependent tunnel coupling. Taking into account these effects requires a substantial extension of our model, perhaps along the lines of Ref. [44]; we leave these considerations for future studies. We also note that the three-dimensional stochastic Gross-Pitaevskii model considered in Ref. [41] could successfully capture the experimentally observed dependence of the relaxation time on the input parameters.

Another source of the discrepancy can come from the definition of the relaxation time. While the damped oscillation in Eq. (V.1) is the low-amplitude approximation of the two-mode model result in Ref. [38], the fitted regime in time is different: instead of the long-living excitations, the experiment focuses on a shorter timescale where the amplitude is still large.

A further question is the proper form of the initial state in the effectively one-dimensional model. For simplicity, following [37, 49] we considered the non-zero mode part of the initial state as a zero (or finite) temperature equilibrium state, while the zero mode realised the initial angle  $\varphi_0$ , which is a coherent state. Considering more realistic initial states that take into account the effect of the preparation procedure by splitting the condensate [35, 36] is left for further study.

Additionally, as discussed at the end of Sec. IV, near the edges of the harmonic longitudinal trap, where the density approaches zero, the field-theoretic approximation is not valid and the Luttinger liquid description breaks down. In our analysis, the Hamiltonian (II.40) used for the simulations is regular (finite) even at the edges; however, the next order interaction (in particle density) would blow up. To avoid unreliable results, we analysed quantities located at the centre and only considered time evolution before revivals appear. Developing a robust method to model the edges requires further analysis.

## VI. CONCLUSIONS

We considered an effective one-dimensional quantum field theory model of the coupled bosonic condensate simulator of quantum sine-Gordon field theory. Previously, experiments established it as a good simulator in equilibrium [27, 31]; however, its non-equilibrium dynamics displayed phase-locking behaviour [38] in contrast to the universal

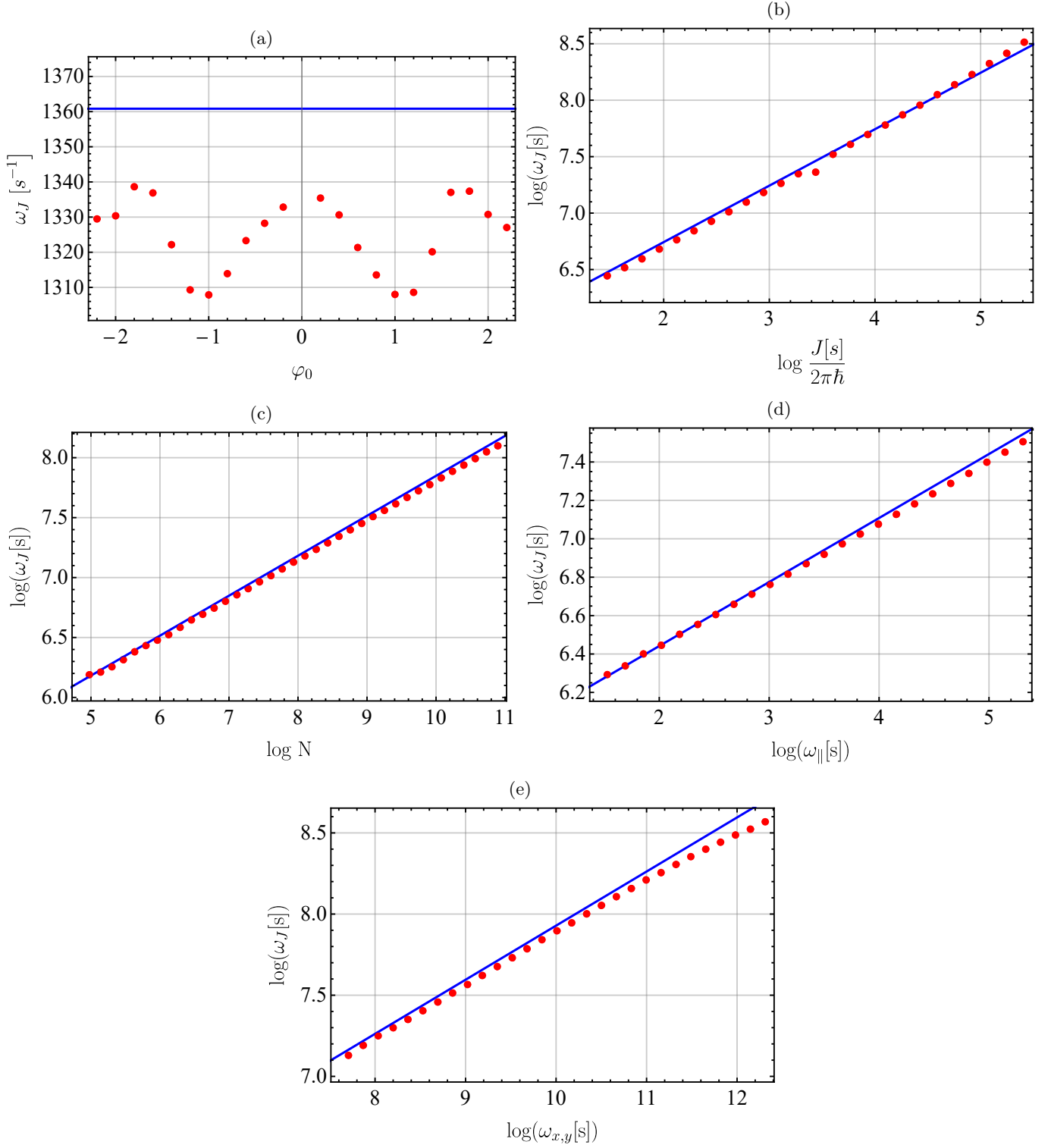


Figure V.4: The Josephson frequency as a function of (a) the initial phase difference  $\varphi_0$ , (b) the Josephson coupling  $J$ , (c) the number of atoms  $N$ , and the strength of (d) the longitudinal and (e) the transversal trapping potential,  $\omega_{\parallel}$  and  $\omega_{\perp}$ . Blue lines indicate the theoretical prediction of the linearised homogeneous model. Parameters:  $T = 0 \text{ nK}$ ,  $\varphi_0 = -1.3(2)$ ,  $N = 3300$ ,  $\sigma_N = 300$ ,  $J/(2\pi\hbar) = 19 \text{ Hz}$ , (e):  $J/(2\pi\hbar) = 30 \text{ Hz}$ .

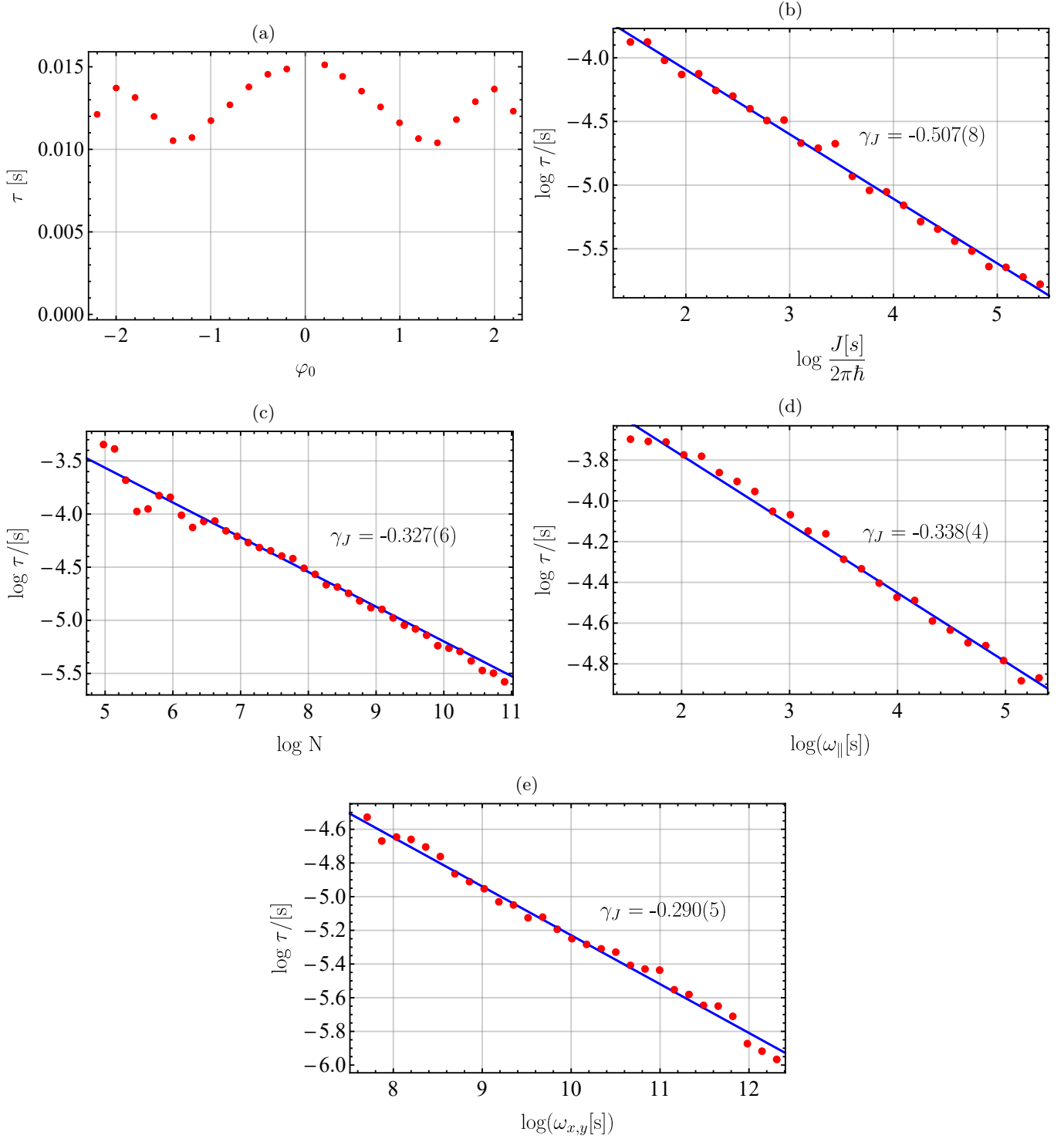


Figure V.5: The relaxation time  $\tau$  as a function of (a) the initial phase difference  $\varphi_0$ , (b) the Josephson coupling  $J$ , (c) the number of atoms  $N$ , and the strength of (d) the longitudinal and (e) the transversal trapping potential,  $\omega_{\parallel}$  and  $\omega_{\perp}$ . We also showed the fitted line (blue) and the corresponding exponent  $\gamma$ . Parameters:  $T = 0$  nK,  $\varphi_0 = -1.3(2)$ ,  $\sigma_N = 300$ ,  $N = 3300$ ,  $J/(2\pi\hbar) = 19.0$  Hz.

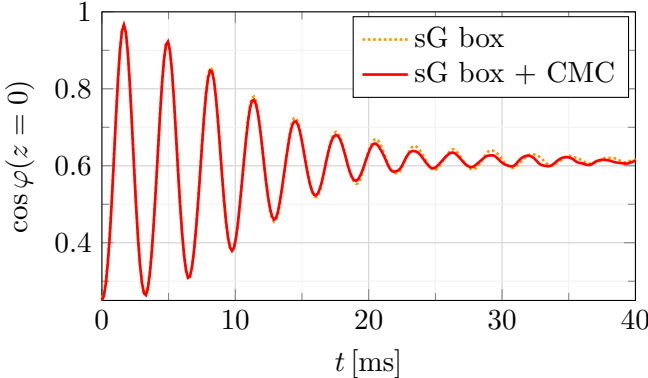


Figure VI.1: Phase relaxation of the pure sine–Gordon model compared to the sine–Gordon dynamics with the common mode coupling (CMC) in a flat-bottom (box) longitudinal trapping potential. (Data is the same as in Fig. III.1.) Parameters:  $N = 3300$ ,  $J/(2\pi\hbar) = 19.0$  Hz,  $T = 0.0$  nK,  $\varphi_0^r = -1.3$ ,  $\sigma_{\varphi_0^r} = 0.2$ ,  $\sigma_N = 0$ .

rephasing predicted from theory [34–37].

We have demonstrated that the phase-locking dynamics can be accounted for by considering the effect of the longitudinal trapping potential. The role of the longitudinal trapping was already found in the stochastic Gross–Pitaevski approach [41]. However, our approach reaches this conclusion in a one-dimensional field theory setting, suggesting that the experiment can be considered as a good simulator of sine-Gordon field theory on an inhomogeneous background. We also found that the coupling between the relative phase (corresponding to the sine-Gordon field) and the average phase (common mode) does not play a significant role in the time interval where boundary effects can be neglected. As a consequence, we fully expect that a box trap prepared by shaping the trapping potential, as proposed in Ref. [61], can achieve an accurate simulation of sine-Gordon dynamics out of equilibrium as illustrated in

Fig. VI.1.

We close by mentioning a few interesting open questions. One of them is to take into account deviations from the strictly one-dimensional behaviour, i.e., 3D effects, which are thought to account for the anomalous scaling of the relaxation time and the Josephson frequency with the number of atoms in the trap. The other is modelling the behaviour near the edges. In the case of the parabolic longitudinal trap, the density of the condensate approaches zero at the edge, which increases the effective coupling to the common mode, thereby calling into question the validity of the field-theoretic model. For a box trap, we expect that the sine-Gordon field satisfies Neumann boundary conditions at the edge, which is an integrable boundary condition with exactly known reflection factors [62] and boundary excitation spectrum [63], which makes it an interesting question whether these predictions can be verified experimentally.

#### ACKNOWLEDGMENTS

We are grateful to J. Schmiedmayer for inspiring discussions and for providing access to some of their unpublished experimental results. This work was supported by the HUN-REN Hungarian Research Network through the Supported Research Groups Programme, HUN-REN-BME-BCE Quantum Technology Research Group (TKCS-2024/34), and also by the National Research, Development and Innovation Office of Hungary (NKFIH) through OTKA Grant No. ANN 142584. The NKFIH also provided partial support to G.T. via the Grant “Quantum Information National Laboratory” with Grant No. 2022-2.1.1-NL-2022-00004. B.F. was also partially supported by the Doctoral Excellence Fellowship Programme (DCEP), funded by the National Research Development and Innovation Fund of the Ministry of Culture and Innovation and the Budapest University of Technology and Economics.

---

- [1] R. P. Feynman, “Simulating physics with computers,” *Int. J. Theor. Phys.* **21** (1982) 467–488.
- [2] J. I. Cirac, P. Maraner, and J. K. Pachos, “Cold Atom Simulation of Interacting Relativistic Quantum Field Theories,” *Phys. Rev. Lett.* **105** (2010) 190403, [arXiv:1006.2975 \[cond-mat.str-el\]](https://arxiv.org/abs/1006.2975).
- [3] T. Kinoshita, T. Wenger, and D. S. Weiss, “A quantum Newton’s cradle,” *Nature* **440** (2006) 900–903.
- [4] S. Hofferberth, I. Lesanovsky, B. Fischer, T. Schumm, and J. Schmiedmayer, “Non-equilibrium coherence dynamics in one-dimensional Bose gases,” *Nature* **449** (2007) 324–327, [arXiv:0706.2259 \[cond-mat.other\]](https://arxiv.org/abs/0706.2259).
- [5] S. Trotzky, Y. A. Chen, A. Flesch, I. P. McCulloch, U. Schollwöck, J. Eisert, and I. Bloch, “Probing the relaxation towards equilibrium in an isolated strongly correlated one-dimensional Bose gas,” *Nat. Phys.* **8** (2012) 325–330, [arXiv:1101.2659 \[cond-mat.quant-gas\]](https://arxiv.org/abs/1101.2659).
- [6] M. Gring, M. Kuhnert, T. Langen, T. Kitagawa, B. Rauer, M. Schreitl, I. Mazets, D. A. Smith, E. Demler, and J. Schmiedmayer, “Relaxation and Prethermalization in an Isolated Quantum System,” *Science* **337** (2012) 1318, [arXiv:1112.0013 \[cond-mat.quant-gas\]](https://arxiv.org/abs/1112.0013).
- [7] T. Langen, R. Geiger, M. Kuhnert, B. Rauer, and J. Schmiedmayer, “Local emergence of thermal correlations in an isolated quantum many-body system,” *Nat. Phys.* **9** (2013) 640–643, [arXiv:1305.3708 \[cond-mat.quant-gas\]](https://arxiv.org/abs/1305.3708).
- [8] F. Meinert, M. J. Mark, E. Kirilov, K. Lauber, P. Weinmann, A. J. Daley, and H. C. Nägerl, “Quantum Quench in an Atomic One-Dimensional Ising Chain,” *Phys. Rev. Lett.* **111** (2013) 053003, [arXiv:1304.2628 \[cond-mat.quant-gas\]](https://arxiv.org/abs/1304.2628).

[9] T. Fukuhara, P. Schauß, M. Endres, S. Hild, M. Cheneau, I. Bloch, and C. Gross, “Microscopic observation of magnon bound states and their dynamics,” *Nature* **502** (2013) 76–79, [arXiv:1305.6598 \[cond-mat.quant-gas\]](https://arxiv.org/abs/1305.6598).

[10] T. Langen, S. Erne, R. Geiger, B. Rauer, T. Schweigler, M. Kuhnert, W. Rohringer, I. E. Mazets, T. Gasenzer, and J. Schmiedmayer, “Experimental observation of a generalized Gibbs ensemble,” *Science* **348** (2015) 207–211, [arXiv:1411.7185 \[cond-mat.quant-gas\]](https://arxiv.org/abs/1411.7185).

[11] M. A. Cazalilla and M. Rigol, “Editorial: Focus on Dynamics and Thermalization in Isolated Quantum Many-Body Systems,” *New J. Phys.* **12** (2010) 055006.

[12] A. Polkovnikov, K. Sengupta, A. Silva, and M. Vengalattore, “Colloquium: Nonequilibrium dynamics of closed interacting quantum systems,” *Rev. Mod. Phys.* **83** (2011) 863–883, [arXiv:1007.5331 \[cond-mat.stat-mech\]](https://arxiv.org/abs/1007.5331).

[13] C. Gogolin and J. Eisert, “Equilibration, thermalisation, and the emergence of statistical mechanics in closed quantum systems,” *Rep. Prog. Phys.* **79** (2016) 056001, [arXiv:1503.07538 \[quant-ph\]](https://arxiv.org/abs/1503.07538).

[14] P. Calabrese, F. H. L. Essler, and G. Mussardo, “Introduction to ‘Quantum Integrability in Out of Equilibrium Systems’,” *J. Stat. Mech.* **6** (2016) 064001.

[15] I. Affleck and M. Oshikawa, “Field-induced gap in Cu benzoate and other  $S = 1/2$  antiferromagnetic chains,” *Phys. Rev. B* **60** (1999) 1038–1056, [arXiv:cond-mat/9905002 \[cond-mat.str-el\]](https://arxiv.org/abs/cond-mat/9905002).

[16] I. Umegaki, H. Tanaka, T. Ono, H. Uekusa, and H. Nojiri, “Elementary excitations of the  $S = 1/2$  one-dimensional antiferromagnet  $\text{KCuGaF}_6$  in a magnetic field and quantum sine-Gordon model,” *Phys. Rev. B* **79** (2009) 184401, [arXiv:0902.1371 \[cond-mat.str-el\]](https://arxiv.org/abs/0902.1371).

[17] S. A. Zvyagin, A. K. Kolezhuk, J. Krzystek, and R. Feyerherm, “Excitation Hierarchy of the Quantum Sine-Gordon Spin Chain in a Strong Magnetic Field,” *Phys. Rev. Lett.* **93** (2004) 027201, [arXiv:cond-mat/0403364 \[cond-mat.str-el\]](https://arxiv.org/abs/cond-mat/0403364).

[18] A. Roy and H. Saleur, “Quantum electronic circuit simulation of generalized sine-Gordon models,” *Phys. Rev. B* **100** (2019) 155425, [arXiv:1902.09530 \[cond-mat.mes-hall\]](https://arxiv.org/abs/1902.09530).

[19] A. Roy, D. Schuricht, J. Hauschild, F. Pollmann, and H. Saleur, “The quantum sine-Gordon model with quantum circuits,” *Nucl. Phys. B* **968** (2021) 115445, [arXiv:2007.06874 \[quant-ph\]](https://arxiv.org/abs/2007.06874).

[20] F. H. L. Essler, H. Frahm, F. Göhmann, A. Klümper, and V. E. Korepin, *The One-Dimensional Hubbard Model*. Cambridge University Press, 2005.

[21] T. Giamarchi, *Quantum physics in one dimension*. Internat. Ser. Mono. Phys. Clarendon Press, Oxford, 2004.

[22] E. Haller, R. Hart, M. J. Mark, J. G. Danzl, L. Reichsöllner, M. Gustavsson, M. Dalmonte, G. Pupillo, and H.-C. Nägerl, “Pinning quantum phase transition for a Luttinger liquid of strongly interacting bosons,” *Nature* **466** (2010) 597–600, [arXiv:1004.3168 \[cond-mat.quant-gas\]](https://arxiv.org/abs/1004.3168).

[23] D. Controzzi, F. H. L. Essler, and A. M. Tsvelik, “Dynamical Properties of one dimensional Mott Insulators,” *arXiv e-prints* (2000) cond-mat/0011439, [arXiv:cond-mat/0011439 \[cond-mat.str-el\]](https://arxiv.org/abs/cond-mat/0011439).

[24] A. B. Zamolodchikov and A. B. Zamolodchikov, “Factorized S-matrices in two dimensions as the exact solutions of certain relativistic quantum field theory models,” *Annals Phys.* **120** (1979) 253–291.

[25] F. A. Smirnov, *Form Factors in Completely Integrable Models of Quantum Field Theory*. World Scientific, 1992.

[26] S. Lukyanov and A. Zamolodchikov, “Exact expectation values of local fields in the quantum sine-Gordon model,” *Nucl. Phys. B* **493** (1997) 571–587, [arXiv:hep-th/9611238 \[hep-th\]](https://arxiv.org/abs/hep-th/9611238).

[27] T. Schweigler, V. Kasper, S. Erne, I. Mazets, B. Rauer, F. Cataldini, T. Langen, T. Gasenzer, J. Berges, and J. Schmiedmayer, “Experimental characterization of a quantum many-body system via higher-order correlations,” *Nature* **545** (2017) 323–326, [arXiv:1505.03126 \[cond-mat.quant-gas\]](https://arxiv.org/abs/1505.03126).

[28] E. Wybo, A. Bastianello, M. Aيدلسبرغر, I. Bloch, and M. Knap, “Preparing and Analyzing Solitons in the Sine-Gordon Model with Quantum Gas Microscopes,” *PRX Quantum* **4** (2023) 030308, [arXiv:2303.16221 \[cond-mat.quant-gas\]](https://arxiv.org/abs/2303.16221).

[29] E. Wybo, M. Knap, and A. Bastianello, “Quantum sine-Gordon dynamics in coupled spin chains,” *Phys. Rev. B* **106** (2022) 075102, [arXiv:2203.09530 \[cond-mat.str-el\]](https://arxiv.org/abs/2203.09530).

[30] V. Gritsev, A. Polkovnikov, and E. Demler, “Linear response theory for a pair of coupled one-dimensional condensates of interacting atoms,” *Phys. Rev. B* **75** (2007) 174511, [arXiv:cond-mat/0701421 \[cond-mat.other\]](https://arxiv.org/abs/cond-mat/0701421).

[31] S. Beck, I. E. Mazets, and T. Schweigler, “Nonperturbative method to compute thermal correlations in one-dimensional systems,” *Phys. Rev. A* **98** (2018) 023613, [arXiv:1802.06610 \[cond-mat.quant-gas\]](https://arxiv.org/abs/1802.06610).

[32] P. Calabrese and J. Cardy, “Time Dependence of Correlation Functions Following a Quantum Quench,” *Phys. Rev. Lett.* **96** (2006) 136801, [arXiv:cond-mat/0601225 \[cond-mat.stat-mech\]](https://arxiv.org/abs/cond-mat/0601225).

[33] P. Calabrese and J. Cardy, “Quantum quenches in extended systems,” *J. Stat. Mech. Theor. Exp.* **2007** (2007) 06008, [arXiv:0704.1880 \[cond-mat.stat-mech\]](https://arxiv.org/abs/0704.1880).

[34] E. G. Dalla Torre, E. Demler, and A. Polkovnikov, “Universal Rephasing Dynamics after a Quantum Quench via Sudden Coupling of Two Initially Independent Condensates,” *Phys. Rev. Lett.* **110** (2013) 090404, [arXiv:1211.5145 \[cond-mat.quant-gas\]](https://arxiv.org/abs/1211.5145).

[35] L. Foini and T. Giamarchi, “Nonequilibrium dynamics of coupled Luttinger liquids,” *Phys. Rev. A* **91** (2015) 023627, [arXiv:1412.6377 \[cond-mat.quant-gas\]](https://arxiv.org/abs/1412.6377).

[36] L. Foini and T. Giamarchi, “Relaxation dynamics of two coherently coupled one-dimensional bosonic gases,” *Eur. Phys. J. Special Topics* **226** (2017) 2763–2774, [arXiv:1612.01858 \[cond-mat.quant-gas\]](https://arxiv.org/abs/1612.01858).

[37] D. X. Horváth, I. Lovas, M. Kormos, G. Takács, and G. Zaránd, “Nonequilibrium time evolution and rephasing in the quantum sine-Gordon model,” *Phys. Rev. A* **100** (2019) 013613.

[38] M. Pigneur, T. Berrada, M. Bonneau, T. Schumm, E. Demler, and J. Schmiedmayer, “Relaxation to a Phase-Locked Equilibrium State in a One-Dimensional Bosonic Josephson Junction,” *Phys. Rev. Lett.* **120** (2018) 173601, [arXiv:1711.06635 \[quant-ph\]](https://arxiv.org/abs/1711.06635).

[39] I. Marino, S. Raghavan, S. Fantoni, S. R. Shenoy, and A. Smerzi, “Bose-condensate tunneling dynamics:

Momentum-shortened pendulum with damping,” *Phys. Rev. A* **60** no. 1, (July, 1999) 487–493.

[40] M. Pigneur and J. Schmiedmayer, “Analytical pendulum model for a bosonic Josephson junction,” *Phys. Rev. A* **98** (2018) 063632, [arXiv:1810.02772 \[quant-ph\]](https://arxiv.org/abs/1810.02772).

[41] J. F. Mennemann, I. E. Mazets, M. Pigneur, H. P. Stimming, N. J. Mauser, J. Schmiedmayer, and S. Erne, “Relaxation in an extended bosonic Josephson junction,” *Phys. Rev. Research* **3** (2021) 023197, [arXiv:2012.05885 \[cond-mat.quant-gas\]](https://arxiv.org/abs/2012.05885).

[42] Y. D. van Nieuwkerk and F. H. L. Essler, “Self-consistent time-dependent harmonic approximation for the sine-Gordon model out of equilibrium,” *J. Stat. Mech. Theor. Exp.* **8** (2019) 084012, [arXiv:1812.06690 \[cond-mat.quant-gas\]](https://arxiv.org/abs/1812.06690).

[43] Y. D. van Nieuwkerk and F. Essler, “On the low-energy description for tunnel-coupled one-dimensional Bose gases,” *Scipost Phys.* **9** (2020) 025, [arXiv:2003.07873 \[cond-mat.quant-gas\]](https://arxiv.org/abs/2003.07873).

[44] Y. D. van Nieuwkerk, J. Schmiedmayer, and F. Essler, “Josephson oscillations in split one-dimensional Bose gases,” *Scipost Phys.* **10** (2021) 090, [arXiv:2010.11214 \[cond-mat.quant-gas\]](https://arxiv.org/abs/2010.11214).

[45] M. J. Steel, M. K. Olsen, L. I. Plimak, P. D. Drummond, S. M. Tan, M. J. Collett, D. F. Walls, and R. Graham, “Dynamical quantum noise in trapped Bose-Einstein condensates,” *Phys. Rev. A* **58** (1998) 4824–4835, [arXiv:cond-mat/9807349 \[cond-mat.soft\]](https://arxiv.org/abs/cond-mat/9807349).

[46] A. Sinatra, C. Lobo, and Y. Castin, “Classical-Field Method for Time Dependent Bose-Einstein Condensed Gases,” *Phys. Rev. Lett.* **87** (2001) 210404, [arXiv:cond-mat/0101210 \[cond-mat.soft\]](https://arxiv.org/abs/cond-mat/0101210).

[47] C. Bodet, J. Estève, M. K. Oberthaler, and T. Gasenzer, “Two-mode Bose gas: Beyond classical squeezing,” *Phys. Rev. A* **81** (2010) 063605, [arXiv:1002.2504 \[cond-mat.quant-gas\]](https://arxiv.org/abs/1002.2504).

[48] D. X. Horváth, I. Lovas, M. Kormos, G. Takács, and G. Zaránd, “Nonequilibrium time evolution and rephasing in the quantum sine-Gordon model,” *Phys. Rev. A* **100** (2019) 013613, [arXiv:1809.06789 \[cond-mat.quant-gas\]](https://arxiv.org/abs/1809.06789).

[49] D. Szász-Schagrin, I. Lovas, and G. Takács, “Nonequilibrium time evolution in the sine-Gordon model,” *Phys. Rev. B* **109** (2024) 014308, [arXiv:2309.03596 \[cond-mat.stat-mech\]](https://arxiv.org/abs/2309.03596).

[50] M. Olshanii, “Atomic Scattering in the Presence of an External Confinement and a Gas of Impenetrable Bosons,” *Phys. Rev. Lett.* **81** (1998) 938–941, [arXiv:cond-mat/9804130 \[cond-mat\]](https://arxiv.org/abs/cond-mat/9804130).

[51] D. S. Shlyapnikov, D. M. Petrov, and G. V. Gangardt, “Low-dimensional trapped gases,” *J. Phys. IV France* **116** (2004) 5–44, [arXiv:cond-mat/0409230 \[cond-mat.stat-mech\]](https://arxiv.org/abs/cond-mat/0409230).

[52] M. A. Cazalilla, “Bosonizing one-dimensional cold atomic gases,” *Journal of Physics B Atomic Molecular Physics* **37** (2004) S1–S47, [arXiv:cond-mat/0307033 \[cond-mat.mes-hall\]](https://arxiv.org/abs/cond-mat/0307033).

[53] M. A. Cazalilla, R. Citro, T. Giamarchi, E. Orignac, and M. Rigol, “One dimensional bosons: From condensed matter systems to ultracold gases,” *Rev. Mod. Phys.* **83** (2011) 1405–1466, [arXiv:1101.5337 \[cond-mat.str-el\]](https://arxiv.org/abs/1101.5337).

[54] A. Polkovnikov, “Quantum corrections to the dynamics of interacting bosons: Beyond the truncated Wigner approximation,” *Phys. Rev. A* **68** (2003) 053604, [arXiv:cond-mat/0303628 \[cond-mat.stat-mech\]](https://arxiv.org/abs/cond-mat/0303628).

[55] A. Polkovnikov, “Phase space representation of quantum dynamics,” *Ann. Phys.* **325** (2010) 1790–1852, [arXiv:0905.3384 \[cond-mat.stat-mech\]](https://arxiv.org/abs/0905.3384).

[56] T. Rakovszky, M. Mestyán, M. Collura, M. Kormos, and G. Takács, “Hamiltonian truncation approach to quenches in the Ising field theory,” *Nucl. Phys. B* **911** (2016) 805–845, [arXiv:1607.01068 \[cond-mat.stat-mech\]](https://arxiv.org/abs/1607.01068).

[57] G. Delfino, “Quantum quenches with integrable pre-quench dynamics,” *J. Phys. A: Math. Theor.* **47** (2014) 402001, [arXiv:1405.6553 \[cond-mat.stat-mech\]](https://arxiv.org/abs/1405.6553).

[58] G. Delfino and J. Viti, “On the theory of quantum quenches in near-critical systems,” *J. Phys. A: Math. Theor.* **50** (2017) 084004, [arXiv:1608.07612 \[cond-mat.stat-mech\]](https://arxiv.org/abs/1608.07612).

[59] B. Bertini, D. Schuricht, and F. H. L. Essler, “Quantum quench in the sine-Gordon model,” *J. Stat. Mech. Theor. Exp.* **2014** (2014) 10035, [arXiv:1405.4813 \[cond-mat.stat-mech\]](https://arxiv.org/abs/1405.4813).

[60] A. Cortés Cubero and D. Schuricht, “Quantum quench in the attractive regime of the sine-Gordon model,” *J. Stat. Mech. Theor. Exp.* **10** (2017) 103106, [arXiv:1707.09218 \[cond-mat.stat-mech\]](https://arxiv.org/abs/1707.09218).

[61] M. Tajik, B. Rauer, T. Schweigler, F. Cataldini, J. Sabino, F. S. Møller, S.-C. Ji, I. E. Mazets, and J. Schmiedmayer, “Designing arbitrary one-dimensional potentials on an atom chip,” *Optics Express* **27** (2019) 33474, [arXiv:1908.01563 \[cond-mat.quant-gas\]](https://arxiv.org/abs/1908.01563).

[62] S. Ghoshal and A. Zamolodchikov, “Boundary S Matrix and Boundary State in Two-Dimensional Integrable Quantum Field Theory,” *Int. J. Mod. Phys. A* **9** (1994) 3841–3885, [arXiv:hep-th/9306002 \[hep-th\]](https://arxiv.org/abs/hep-th/9306002).

[63] Z. Bajnok, L. Palla, and G. Takács, “Boundary states and finite size effects in sine-Gordon model with Neumann boundary condition,” *Nucl. Phys. B* **614** (2001) 405–448, [arXiv:hep-th/0106069 \[hep-th\]](https://arxiv.org/abs/hep-th/0106069).

## Appendix A: Summary of model parameters

In this appendix, we summarise all the parameters of our model. It is important to precisely separate the input parameters that are varied independently, and to determine all the physical characteristics of the system.

Input parameters of the experiment (which are directly given or can be tuned):

- atomic mass  $m$  (for  $^{87}\text{Rb}$ ,  $m = 86.90918 \cdot 1.660539 \cdot 10^{-27} = 1.44316 \cdot 10^{-25} \text{ kg}$ ),
- one-dimensional interaction strength  $g_{1\text{D}} \approx 2\hbar\omega_{\perp}a_s$  (for  $^{87}\text{Rb}$ ,  $a_s = 5.24 \text{ nm}$ , and for the experimental setup considered,  $\omega_{\perp} = 2\pi \cdot 1500 \text{ Hz}$ ),
- total number of atoms  $N$  (typically between 750 and 4500) and its uncertainty  $\sigma_N$  (if its known),
- longitudinal trapping potential  $\omega_{\parallel}$  (for the experimental setup considered,  $\omega_{\perp} = 2\pi \cdot 12 \text{ Hz}$  if not indicated otherwise),
- Josephson coupling  $\tilde{J} = J/(2\pi\hbar)$ ,
- the initial total relative phase  $\varphi_0^r$  and its standard deviation  $\sigma_{\varphi_0^r}$ ,
- temperature  $T$  (the temperature of the experimental condensate is 18 nK before the splitting procedure; however, as argued in Section III B 1, the relative degrees must be substantially colder, therefore we chose the temperature as 0).

These input parameters determine the physical system, and they can be changed independently. From these, we can calculate many other physical quantities relevant to our study, such as

- length of the condensate  $L$ ,
- 1D density at the midpoint ( $z = 0$ ):  $n_0$ ,
- sound velocity at the midpoint:  $c_0$ ,
- Luttinger parameter at the midpoint:  $K_0$ ,
- chemical potential,  $\mu$ ,
- Josephson frequency,  $\omega_J$ .

The relations determining these parameters are given by

$$\begin{aligned} L &= \left( \frac{6g_{1\text{D}}N}{m\omega_{\parallel}^2} \right)^{1/3}, \\ n_0 &= \frac{3^{2/3}}{2^{7/3}} \left( \frac{m\omega_{\parallel}^2 N^2}{g_{1\text{D}}} \right)^{1/3}, \\ c_0 &= \frac{3^{1/3}}{2^{7/6}} \left( \frac{g_{1\text{D}}N\omega_{\parallel}}{m} \right)^{1/3}, \\ K_0 &= \pi\hbar \frac{3^{1/3}}{2^{7/6}} \left( \frac{N\omega_{\parallel}}{mg_{1\text{D}}^2} \right)^{1/3}, \\ \mu &= \left( \frac{3^2}{2^7} g_{1\text{D}}^2 N^2 \omega_{\parallel}^2 m \right)^{1/3}, \\ \omega_J &= 2\pi \left( \frac{3^2 \tilde{J}^3 N^2 g_{1\text{D}}^2 \omega_{\parallel}^2 m}{2^4 \pi^3 \hbar^3} \right)^{1/6}. \end{aligned} \quad (\text{A.1})$$

The following relations are also convenient:

$$\begin{aligned} R_{\text{TF}}^2 &= \frac{2\mu}{m\omega_{\parallel}^2}, \\ n_0 &= \frac{\mu}{g_{1\text{D}}}, \\ N &= \frac{4}{3} n_0 R_{\text{TF}}, \\ \mu &= \left( \frac{3}{4} g_{1\text{D}} N \sqrt{\frac{1}{2} m \omega_{\parallel}^2} \right)^{2/3}, \\ m &= \frac{\pi\hbar n_0}{K_0^0 c_0}, \\ N_s &= \left[ \frac{3^{2/3}}{2^{5/6}} \left( \frac{m g_{1\text{D}}^2 N^2}{\omega_{\parallel} \hbar^3} \right)^{1/3} \right], \\ g &= 2\pi \tilde{J} \frac{2^{3/2}}{\omega_{\parallel}}, \\ g_{1\text{D}} &= \frac{\pi\hbar c_0}{K_0}. \end{aligned} \quad (\text{A.2})$$

The lattice parameters are chosen according to

$$\begin{aligned} N_s &= \left[ \frac{L m c_0}{\hbar} \right], \\ a &= \frac{L}{N_s}, \end{aligned} \quad (\text{A.3})$$

so the lattice constant satisfies

$$a \approx \frac{\hbar}{m c_0}. \quad (\text{A.4})$$